1    **Soil-landscape relationship in sandstone-gneiss topolithosequence in Amazonas, Brazil**

2    Julimar da Silva Fonseca[1], Milton César Costa Campos[1], Elilson Gomes de Brito Filho[1]*, Bruno Campos

3    Mantovanelli[2], Laércio Santos Silva[3], Alan Ferreira Leite de Lima[1], José Maurício Da Cunha[1], Emily Lira

4    Simões[1], Luís Antônio Coutrim dos Santos[1]

5    [1]Universidade Federal do Amazonas - UFAM, Instituto de Educação, Agricultura e Ambiente, Humaitá,

6    Amazonas, Brasil

7    [2]Universidade Federal de Santa Maria - UFSM, departamento de agronomia, Santa Maria, Rio Grande do Sul,

8    Brasil.

9    [3]Universidade Estadual Paulista - UNESP, departamento de agronomia, Jaboticabal, São Paulo, Brasil.

10    *Corresponding author: Elilson Gomes de Brito Filho, Instituto de Educação, Agricultura e Ambiente –

11    Universidade Federal do Amazonas (UFAM), Humaitá, Amazonas, Brasil, Zip code: 69800-000, telephone:

12    +5597981121704, e-mail: bfsambiente@gmail.com.

## 1 Abstract

Soil position in the landscape reveals its history of formation and genesis. Therefore, the landscape is the combination of features of the surface of the earth with subsurface components (parent material), while the soil is a three-dimensional, dynamic natural body inserted in the landscape. This research aimed to study the soil-landscape relationship in a sandstone-gneiss topolithosequence in Amazonas, Brazil. The study was carried out along a 9.253-meter transect from the top downwards the softer slope. Soil profiles were selected in five landscape compartments (top, upper third, lower third, transport foothill, and deposition foothill). Morphological, mineralogical, physical, chemical, and ray diffraction characterizations were performed. Soils had different morphological, physical, chemical, and mineralogical attributes due to the variations of the geological substrate and landscape position. The mineralogy of the clay fraction is composed of kaolinite, goethite, hematite, and gibbsite, with goethite being the predominant iron oxide. A sand fraction dominance was observed in relation to the other fractions in all the profiles, being related to the alluvial nature of the parent material, with the highest values occurring in the lower third. The separation of the landscape into geomorphic surfaces and identification of the parent material were effective for understanding the variation of soil attributes along the landscape.

## 2 Introduction

The soil is the product of the combinations of factors and processes of formation governed by the local conditions of its occurrence. The intensity of these factors and processes promote progressive transformations in the parent material, which over time are expressed by morphological, chemical, physical, and mineralogical soil properties. Thus, considering the Amazonian environments, climate conditions of high temperature and high precipitation prevail in the Brazilian Amazon, favoring an intense mineral weathering and, therefore, the formation of soils with predominant characteristics (Dalamerlinda et al., 2017). For this reason, it is necessary to recognize the interaction among these factors and their role in soil formation (Campos et al., 2012a; Silva, 2016).

Soil position in the landscape reveals its history of formation and genesis (Campos et al., 2011). Thus, the landscape is the combination of features of the surface of the earth with subsurface components (parent material), while the soil is a three-dimensional, dynamic natural body inserted in the landscape (Minasny and Mcbratney, 2006). In general, soil attributes present the characteristics of the matrix rock, but at a local scale,

41 the occurrence of attributes can be very different due to the existence of more lithologic substrate or even the

42 predominance of a specific formation process (Campos et al., 2012a). Thus, the relief, although considered a

43 supporting factor, acts on the spatial distribution of soil attributes, water dynamics, presence of unconsolidated

44 sediments, pedogenetic development, and processes that translate into the most varied soil types (Bockheim et

45 al., 2005; Vasconcelos et al., 2012; LI et al., 2015).

46 For a better understanding of the soils in the landscape, the preconized concepts of the soil-landscape

47 relationship become necessary as criteria for understanding the spatiotemporal variability of soil attributes and

48 visualization of dynamic processes such as the transport of water, solutes, and sediments (Sommer, 2006;

49 Campos et al., 2011). Despite the great representation of the Middle Madeira River region, the most common

50 physiographic environments are floodplains, native fields, and transition areas, which are dominated by

51 Inceptisols, Ultisols, and Entisols, thus showing the main characteristic of the Amazon region as a function of

52 the exuberant grouping of landscapes associated with different soil classes in a short space of geographical

53 position (Campos et al., 2012a; Campos et al., 2012b).

54 The direct effects of the composition of the parent material have been studied in the literature. Montanari et al.

55 (2010) found the dominance of goethite and kaolinite in a concave landform in relation to linear and convex

56 landforms, while the highest hematite contents occurred in linear landforms. Curi and Franzmeier (1984)

57 studied a toposequence of Oxisols and found higher gibbsite concentration in the highest landscape position

58 and kaolinite in the lowest positions associated with goethites of lower mean crystal diameter. All these

59 investigations reinforce the importance of characterizing soil mineralogy to reinforce the relationship between

60 the landscape and parent material, especially Fe and Al oxides because their formation is influenced by

61 environmental conditions and persist for a long time in the soil (Kämpf and Curi, 2000).

62 Despite the long territorial extension of the Amazon region, studies have been conducted and various

63 characteristics and peculiarities of its landscape have revealed new directions in studies on the soil-landscape

64 relationship. Thus, the properties of the soil-landscape relationship associated with the behavior of parent

65 material transmit records of the intensity of pedogenetic processing conditions that prevailed in the

66 environment that influenced the formation of these soils. Therefore, this research aimed to study the soil-

67 landscape relationship in a sandstone-gneiss topolithosequence in mazonas, Brazil.

68 **3 Material and methods**

### 3.1 Characterization of the physical environment

The study area is located at BR 230 km 150 – Transamazônica, municipality of Manicoré, AM – direction of Machadinho do Oeste, RO, at Rodovia do Estanho km 14, located between the geographical coordinates 08°08′12.6″ S and 61°50′06.5″ W (Figure 1). According to the Köppen classification, the regional climate is classified as Am, i.e. a rainy tropical climate (monsoon rains), with a dry period of short duration, temperatures varying from 25 to 27 °C, and annual precipitation of 2,500 mm with the rainy season beginning in October and extending until June and relative air humidity between 85 and 90%.
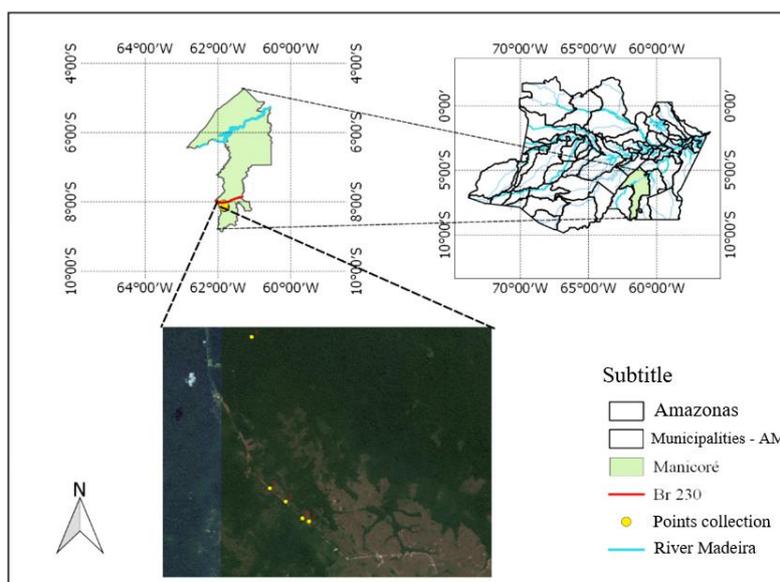
Figure 1. Location of the profiles studied in the municipality of Manicoré in the state of Amazonas, Brazil. Source: ©Google Maps.

Relief configuration is marked by the presence of plateaus in the highest parts, which exhibit flat topographic surfaces, with the border area marked by aligned hills and ridges, while the lower areas constitute a pediplanated surface, locally interrupted by flat top hills (CPRM, 2001).

Regarding the geology, the study area is located on Rondonian Granites characterized by the presence of muscovite, biotite, adamelites, and granodiorites of intrusive cratogenic origin, in the form of stocks and batholiths (BRASIL, 1978). According to ZEE (2008), regional soils are Oxisols. The characteristic vegetation of this region is a dense tropical forest consisting of densified and multi-layered trees between 20 and 50 meters in height (figure 2).

87

88    Figure 2. Images of the collection environment.

89    **3.2 Field methodology**

90    The study was carried out along a 9.253-meter transect from the top downwards the softer slope to the

91    deposition foothill. Measurements of the altitudes were carried out along this transect to make the altimetric

92    profile. Based on the model of Dalrymple et al. (1968), hillside segments were identified mainly based on the

93    variation of the terrain slope (Figure 3).
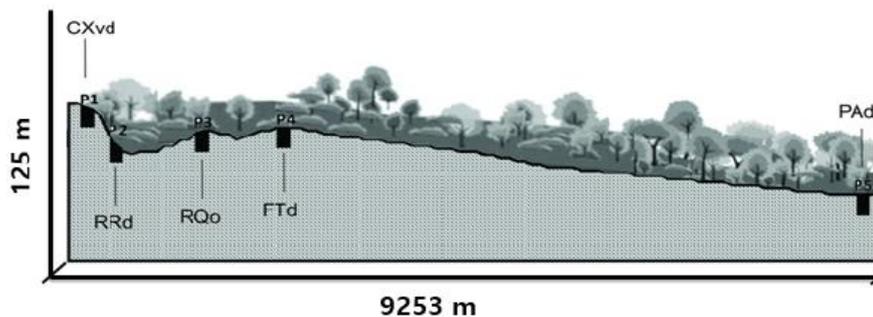
94

95    Figure 3. Schematic profile of the terrain topography and trench position in the topolithosequence in

96    Amazonas, Brazil.

97    Five trenches were opened along the hillside topography following the transect illustrated in Figure 3 in order

98    to characterize the soils, as follows: top (08°08′46.0″ S and 61°49′25.1″ W), upper third (08°08′41.8″ S and

99    61°49′33.9″ W), lower third (08°08′18.3″ S and 61°49′56.3″ W), transport foothill (08°07′59.6″ S and

100   61°50′17.4″ W), and deposition foothill (08°07′59.6″ S and 61°50′17.4″ W). The identification of horizons

101   and morphological description, followed by the sampling of soil horizons, were performed according to Santos

102   et al. (2013). Soils were classified according to criteria established by the Brazilian Soil Classification System

103   (Santos et al., 2013).

104   Twenty samples were collected at different soil profiles: Top: A – 0.0–0.16 m and AB – 0.16–0.30 m; upper

105   third: A – 0.0–0.12 m and ACr – 0.10–0.20 m; lower third: A – 0.0–0.7 m and C1 – 0.15–0.33 m; transport

106 foothill: A – 0.0–0.18 m and AB – 0.18–0.33 m; and deposition foothill: A – 0.0–0.18 m and AB – 0.18–0.32

107 m. The criterion for choosing the depths was the coincidence with surface and subsurface diagnostic horizons.

108 **3.3 Particle size analysis**

109 Particle size analysis was performed by the pipette method using a 0.1 mol L$^{-1}$ NaOH solution as a chemical

110 dispersant and mechanical stirring in a low rotation apparatus for 16 h (Donagema et al., 2017). The clay

111 fraction was separated by gravitational sedimentation, the coarse and fine sand fraction by sieving, and the silt

112 fraction was calculated by difference.

113 **3.4 Chemical analysis**

114 Soil pH was determined in water and 1.0 mol L$^{-1}$ KCl solution in the soil to solution ratio of 1:2.5 (Donagema

115 et al., 2017). The exchangeable cations $Ca^{2+}$, $Mg^{2+}$, and $Al^{3+}$ were extracted with 1.0 mol L$^{-1}$ KCl and measured

116 by atomic absorption spectroscopy. The hydrogen ion and $Al^{3+}$ were extracted with 0.5 mol L$^{-1}$ calcium acetate

117 at pH 7.0 and determined by titration (0.025 mol L$^{-1}$ NaOH) (Donagema et al., 2017). Organic carbon was

118 determined by the wet oxidation method (Walkley and Black, 1934).

119 Bioavailable particulate phosphorus (Pbp) was determined by extraction with anion exchange resin (AER).

120 The principle of phosphorus extraction by AER is its continuous removal from the solution by the exchange

121 with bicarbonate of the resin, creating a concentration gradient that forces the exit of the surface of colloids

122 until an electrochemical equilibrium is reached between the soil and AER (Skogley and Dobermann, 1996).

123 For this, the methodology developed by Kroth (1998) was used as follows: 0.5 g of soil (1 mm) was added in

124 15 mL falcon tubes containing 10 mL distilled water and a sheet of AER saturated with 0.5 mol L$^{-1}$ NaHCO₃.

125 These tubes were stirred for 16 hours on an end-over-end stirrer (33 rpm). The sheets were removed and

126 washed with distilled water jets and then diluted in 10 mL 0.5 mol L$^{-1}$ HCl. The tubes remained uncapped for

127 90 minutes and then closed and stirred for 30 minutes in a horizontal stirrer. Subsequently, a 3 mL aliquot was

128 taken from the extract to determine the P content according to Murphy and Riley (1962). The sum of bases

129 (SB), cation exchange capacity (CEC), base saturation (V), and aluminum saturation (m) were calculated based

130 on the results of the chemical analyses.

131 **3.5 Mineralogical analysis**

132 The minerals of the clay fraction hematite (Hm), goethite (Gt), kaolinite (Kt), and gibbsite (Gb) were

133 characterized by X-ray diffractometry using the powder method after the concentration of iron oxides by

134    boiling the clay fraction in NaOH (Norrish and Taylor, 1961) and deferrifying it by the method of Mehra and

135    Jackson (1960). The samples were diffracted with scanning speed of $1°$ $2θ$ $min^{-1}$ using a Mini-Flex Rigaku II

136    (20 mA, 30 kV) equipped with Cu Kα radiation. The Hm/(Gt+ Hm) ratio was estimated by comparing the peak

137    areas from the Hm/(Gt+Hm) with the proportions of relationships obtained from standard Gt–Hm mixtures.

138    The percentages of Hm and Gt were calculated by allocating the difference between Fed and Feo to these

139    oxides. The Kt/(Kt+Gb) ratio was calculated by peak areas of Gb (002) and Kt (001) reflections. The

140    calculation of the content of isomorphic substitution of iron by aluminum in Gt was obtained by the equation

141    mol $mol^{-1}$ = 1730 − 572 c (Schulze, 1984). For the calculation of the content of isomorphic substitution of iron

142    by aluminum in Hm, the equation mol $mol^{-1}$ = 3098.8 − 615.12 a0 (Schwertmann et al., 1989) was used. The

143    specific surface area (SSA) of Gt was estimated by the formula SSA (Gt) = $(1049/MCD gt 100)^{-5}$ (m$^2$ g$^{-1}$),

144    according to Schulze and Schwertmann (1984), MCD100 = MCD (110) × 0.42 nm (Kämpf, 1981), and the

145    SSA of Hm was estimated by the formula SSA (Hm) = 2 × (r + h) × d (m$^2$ g$^{-1}$), according to (Schwertmann

146    and Kämpf, 1985). The mean crystal diameter (MCD) of Hm and Gt was calculated from the width at half-

147    height (WHH) and the position of mineral reflections using the Scherrer equation (Klug and Alexander, 1974).

148    **4 Results**

149    **4.1 Soil distribution in the landscape**

150    A physiognomy formed by plains was observed in this locality due to the minimal variation of relief. This

151    characteristic is typical in Amazonian environments probably because of the gradual transition action that

152    occurs between fields and the forest in this region. The lowest terrain position is colonized by small shrub

153    species, where there are flood conditions at certain times of the year. Dalrymple et al. (1968) established

154    hypothetical units of hillsides, which may be partially absent or repeated along them. In this study, five hillside

155    segments were identified and mapped in a representative toposequence of the region (Figure 3).

156    The first three hillside segments of the landscape, represented by the top, upper third, and lower third, with

157    elevations from 120 to 125 m, are grouped similarly among each other. This position in the landscape does not

158    confer greater stability to soil attributes, mainly due to the classification of these soils, thus evidencing the

159    total influence of the landscape on its attributes. The third segment is the transport foothill (119 m), with a

160    residual erosional character, starting from the edges of the lower third and showing a slightly sloping

161    conformation to the fifth segment, which may have been formed by relief microvariations of the previous

162   segment. Finally, the fifth segment is the deposition foothill, which presents lower altitudes than the top

163   (between 114 and 116 m), but with different topographic characteristics. In this case, it may be considered a

164   stable geomorphic environment.

165   The pedogenesis of these soils evidences the action of more than one parent material since the partition is

166   composed of five distinct classes in the different segments. Considering that these classes were developed on

167   different sandstone-gneiss parent materials, they are the main cause of alterations in soil attributes at different

168   magnitudes. As observed by Marques Júnior and Lepsch (2000) and Campos (2012c), understanding the

169   different parent materials in a landscape favor the understanding of the variability of soil attributes, thus

170   indicating that geology provides subsidies to explain the local relief and soil behavior.

171   **4.2 Morphological and textural attributes**

172   The genesis and classification showed that all profiles have a moderate diagnostic surface A horizon (Table

173   1). The topographic position of the top showed an incipient subsurface diagnostic B horizon, with no evidence

174   of predominant pedogenic process, being classified as a leptic Dystrophic Ta Haplic Cambisol.

175   Soils of the upper and lower third are poorly evolved, consisting of mineral material or organic material lower

176   than 20 cm thick, with no type of diagnostic B horizon. In the upper third, the soil was characterized as a

177   Regolithic Neosol because it is in a lytic contact at a depth higher than 50 cm and A horizon overlying C or Cr

178   horizon, presenting altered primary minerals, with gravels from the ACr horizon at a depth of 12–35 cm and

179   presence of fragments of semi-weathered rocks (Santos et al., 2013). On the same surface, there was the

180   presence of Quartzarenic Neosol (lower third), soils with no lytic contact within 50 cm of depth, with sequences

181   of A–C horizons, but showing a sand or loamy sand texture in all horizons up to at least 150 cm, mainly

182   consisting of quartz with coarse and fine sand fractions and whitish colors (Santos et al., 2013).

183   The transport foothill, submitted to a higher influence of seasonal variations of the water table, presented

184   mottles in the subsurface horizons of a reddish color, with a small size and distinct contrast. Associated with

185   the mottled color is the presence of plinthite and petroplinthite in amounts varying from common to abundant,

186   corresponding to values between 15 and 40% of the soil volume. These attributes indicate the occurrence of

187   the plinthization pedogenic process, being a diagnostic character of the plinthic horizon, according to the

188   Brazilian Soil Classification System (SiBCS) (Santos et al., 2013). From the attributes and identified horizons,

189   the profile was classified, at suborder level, as an 3.3 Argiluvic Plinthosol.

190    In this segment, there was the presence of an abruptic Dystrophic Yellow Argisol (deposition foothill),

191    presenting textural B horizon and predominance of colors with hue 10 YR and 7.5 YR in the first 100 cm of

192    the B horizon. In this soil, the slope was determinant for the selective removal of clay, contributing to the

193    formation of a textural gradient. In summary, the mineralogical, physical, and chemical results of the

194    characterized profiles accurately elucidated the characteristics of the sandstone-gneiss rock that originated the

195    soils along the topolithosequence.

196    Soil colors ranged from very dark grayish brown to dark brown in the surface horizons (Table 1). Thus, a clear

197    differentiation was observed for subsurface horizons that have colors from yellowish brown to very pale

198    brown. The grayish tones were observed in most horizons, being this coloration associated with a low

199    concentration of iron oxides and predominance of light-colored minerals such as kaolinite and quartz in the

200    sand fraction (EMBRAPA, 2013). This behavior can be verified in Table 3, which shows the predominance of

201    goethite in all profiles, even in the Plinthosol, which showed higher increases of hematite.

202    Surface horizons had the predominance of a weak, small, medium to large structure in the composition of the

203    top and foothill (Table 1). On the other hand, in transport and deposition foothills predominated a moderate,

204    medium, coarse to large structure. According to Silva et al. (2001), the soil drainage, conditioned by the

205    topographic position, has a strong relationship with the type of structure because moderately to well-drained

206    soils tend to have granular or angular and subangular blocky structures, while poorly to imperfectly drained

207    soils tend to exhibit a standard structure in polygonal prisms. Campos et al. (2012a) observed that the relief

208    conditions influenced several soil attributes, considering that the slope creates a complex pattern of transport

209    of water and solutes, acting mainly on soil profile development.

210    The surface horizon of all profiles presented a sandy loam textural class, except for Neosols, which presented

211    a sandy constitution (Table 1). The dominance of the sand fraction in the profiles is explained by the parent

212    material, composed of sandstones of the Palmeiral Formation and Nova Campo Verde Complex. However, the

213    increase in the clay fraction in the Argisol from the Bt1–Bt2–Btf horizon stood out. As highlighted by Campos

214    et al. (2011) and verified in our study, Argisol and Plinthosol seem to have undergone a process of rejuvenation

215    due to their position in the landscape, with a probable loss of clay from the surface horizons, resulting in an

216    abrupt textural change.

217

218  TABLE 1. Morphological and granulometric attributes of a topolithosequence in Amazonas, Brazil.

| Horizon | Depth | Color | Texture | Structure | Clay | Silt | Fine sand | Coarse sand | Total sand | S/C |
|---|---|---|---|---|---|---|---|---|---|---|
| Top – Leptic Dystrophic Ta Haplic Cambisol – CXvd | | | | | | | | | | |
| A | 0–16 | 10 YR 3/2 | Sandy loam | weak, small, granular | 128 | 182 | 386 | 304 | 690 | 1.43 |
| AB | 16–30 | 10 YR 3/2 | Sandy loam | moderate to medium, angular and subangular blocks | 132 | 198 | 393 | 277 | 670 | 1.50 |
| Bi | 30–55 | 10 YR 4/6 | Sandy loam | weak, medium, angular and subangular blocks | 139 | 213 | 416 | 232 | 648 | 1.53 |
| BCr | 55–78+ | 10 YR 4/4 | Sandy loam | weak, small to medium, granular | 142 | 212 | 422 | 224 | 646 | 1.49 |
| Upper third – Leptic Dystrophic Regolithic Neosol – RRd | | | | | | | | | | |
| A | 0–12 | 10 YR 3/2 | Sandy loam | weak, small, granular | 118 | 141 | 241 | 500 | 741 | 1.19 |
| ACr | 12–35 | 10 YR 4/6 | Sandy loam | weak, small, angular and subangular blocks | 111 | 159 | 269 | 460 | 730 | 1.43 |
| Cr/Bi | 35–62 | 10 YR 6/6 | Sandy loam | weak, small, angular and subangular blocks | 116 | 161 | 289 | 441 | 723 | 1.33 |
| Lower third – Typic Orthic Quartzarenic Neosol – RQo | | | | | | | | | | |
| A | 0–15 | 10 YR 3/2 | Sand | weak, small to medium, granular | 56 | 53 | 62 | 829 | 891 | 0.94 |
| C1 | 15–33 | 10 YR 7/2 | Sandy loam | weak, large, angular and subangular blocks | 50 | 61 | 121 | 768 | 889 | 1.21 |
| C2 | 33–50 | 10 YR 7/3 | Loamy sand | moderate, medium to large, angular and subangular blocks | 49 | 87 | 130 | 734 | 864 | 1.78 |
| C3 | 50–75 | 10 YR 7/3 | Loamy sand | moderate, medium to large, angular and subangular blocks | 59 | 88 | 83 | 770 | 853 | 1.49 |
| Cr | 75–105+ | 10 YR 6/4 | Loamy sand | moderate, medium to large, angular and subangular blocks | 53 | 98 | 126 | 723 | 849 | 1.86 |
| Transport foothill – Typic Dystrophic Argiluvic Plinthosol – FTd | | | | | | | | | | |
| A | 0–18 | 10 YR 2/1 | Sandy loam | moderate, medium to large, granular | 131 | 306 | 413 | 150 | 563 | 2.32 |
| AB | 18–33 | 10 YR 3/2 | Sandy loam | weak, medium to large, angular and subangular blocks | 146 | 329 | 467 | 58 | 525 | 2.26 |
| BAf | 33–48 | 10 YR 4/6 | Loam | weak to moderate, small to medium, angular and subangular blocks | 205 | 336 | 435 | 24 | 459 | 1.64 |
| Bf | 48–70 | 10 YR 5/6 | Loam | strong, large, angular and subangular blocks | 257 | 360 | 362 | 21 | 383 | 1.41 |
| BCr | 70–110+ | 10 YR 6/4 | Loam | strong, medium to large, angular and subangular blocks | 258 | 297 | 432 | 13 | 445 | 1.15 |
| Deposition foothill – Abruptic Dystrophic Yellow Argisol – Pad | | | | | | | | | | |
| A1 | 0–18 | 10 YR 5/6 | Sandy loam | weak, small to large, granular | 99 | 146 | 406 | 349 | 755 | 1.49 |
| A2 | 18–32 | 10 YR 5/6 | Sandy loam | moderate, medium to large, angular and subangular blocks | 99 | 172 | 415 | 314 | 729 | 1.73 |
| AB | 32–49 | 10 YR 5/6 | Sandy loam | strong, medium to large, angular and subangular blocks | 95 | 205 | 416 | 284 | 700 | 2.15 |
| Bt1 | 49–74 | 10 YR 6/8 | Clay | strong, medium to large, angular and subangular blocks | 548 | 218 | 188 | 47 | 234 | 0.40 |
| Bt2 | 74–110 | 10 YR 6/4 | Clay | strong, large to very large, angular and subangular blocks | 558 | 228 | 189 | 26 | 215 | 0.41 |
| Btf | 110–125 | 10 YR 6/8 | Clay | strong, large to very large, angular and subangular blocks | 563 | 230 | 202 | 5 | 207 | 0.41 |

219  S/C: silt to clay ratio.

220   Soils of the upper and lower third are poorly evolved, consisting of mineral material or organic material lower

221   than 20 cm thick, with no type of diagnostic B horizon. In the upper third, the soil was characterized as a

222   Regolithic Neosol because it is in a lytic contact at a depth higher than 50 cm and A horizon overlying C or

223   Cr horizon, presenting altered primary minerals, with gravels from the ACr horizon at a depth of 12–35 cm

224   and presence of fragments of semi-weathered rocks (Santos et al., 2013). On the same surface, there was the

225   presence of Quartzarenic Neosol (lower third), soils with no lytic contact within 50 cm of depth, with

226   sequences of A–C horizons, but showing a sand or loamy sand texture in all horizons up to at least 150 cm,

227   mainly consisting of quartz with coarse and fine sand fractions and whitish colors (Santos et al., 2013).

228   The transport foothill, submitted to a higher influence of seasonal variations of the water table, presented

229   mottles in the subsurface horizons of a reddish color, with a small size and distinct contrast. Associated with

230   the mottled color is the presence of plinthite and petroplinthite in amounts varying from common to abundant,

231   corresponding to values between 15 and 40% of the soil volume. These attributes indicate the occurrence of

232   the plinthization pedogenic process, being a diagnostic character of the plinthic horizon, according to the

233   Brazilian Soil Classification System (SiBCS) (Santos et al., 2013). From the attributes and identified horizons,

234   the profile was classified, at suborder level, as an 3.3 Argiluvic Plinthosol.

235   In this segment, there was the presence of an abrupt Dystrophic Yellow Argisol (deposition foothill),

236   presenting textural B horizon and predominance of colors with hue 10 YR and 7.5 YR in the first 100 cm of

237   the B horizon. In this soil, the slope was determinant for the selective removal of clay, contributing to the

238   formation of a textural gradient. In summary, the mineralogical, physical, and chemical results of the

239   characterized profiles accurately elucidated the characteristics of the sandstone-gneiss rock that originated the

240   soils along the topolithosequence.

241   Soil colors ranged from very dark grayish brown to dark brown in the surface horizons (Table 1). Thus, a clear

242   differentiation was observed for subsurface horizons that have colors from yellowish brown to very pale

243   brown. The grayish tones were observed in most horizons, being this coloration associated with a low

244   concentration of iron oxides and predominance of light-colored minerals such as kaolinite and quartz in the

245   sand fraction (EMBRAPA, 2013). This behavior can be verified in Table 3, which shows the predominance of

246   goethite in all profiles, even in the Plinthosol, which showed higher increases of hematite.

247   Surface horizons had the predominance of a weak, small, medium to large structure in the composition of the

248   top and foothill (Table 1). On the other hand, in transport and deposition foothills predominated a moderate,

249   medium, coarse to large structure. According to Silva et al. (2001), the soil drainage, conditioned by the

250   topographic position, has a strong relationship with the type of structure because moderately to well-drained

251   soils tend to have granular or angular and subangular blocky structures, while poorly to imperfectly drained

252   soils tend to exhibit a standard structure in polygonal prisms. Campos et al. (2012a) observed that the relief

253   conditions influenced several soil attributes, considering that the slope creates a complex pattern of transport

254   of water and solutes, acting mainly on soil profile development.

255   The surface horizon of all profiles presented a sandy loam textural class, except for Neosols, which presented

256   a sandy constitution (Table 1). The dominance of the sand fraction in the profiles is explained by the parent

257   material, composed of sandstones of the Palmeiral Formation and Nova Campo Verde Complex. However,

258   the increase in the clay fraction in the Argisol from the Bt1–Bt2–Btf horizon stood out. As highlighted by

259   Campos et al. (2011) and verified in our study, Argisol and Plinthosol seem to have undergone a process of

260   rejuvenation due to their position in the landscape, with a probable loss of clay from the surface horizons,

261   resulting in an abrupt textural change.

262   In general, the profiles of the soil-landscape relationships presented morphological variations among each

263   other, being the result of a variety of pedogenetic factors and processes. Ribeiro et al. (2012) indicated that the

264   morphological characteristics are due to the soil constitution and conditions under which it was formed,

265   allowing making inferences on pedogenetic processes and environmental conditions, as well as interpreting or

266   predicting the plant behavior and the response of management practices.

267   Particle size composition showed a predominance of the sand fraction over the other fractions, with contents

268   from 207 and 891 g kg$^{-1}$ (Table 1). These characteristics can be explained by the parent material (sandstone),

269   which presented in their constitution predominance of quartz. These high values of total sand are in accordance

270   with Schiavo et al. (2010), who characterized and classified soils developed from sandstones of the

271   Aquidauana Formation.

272   In the A horizon, silt contents ranged from 53 to 306 g kg$^{-1}$, with an increment in depth (Table 1). Low values

273   are associated with young soils still in the formation process. In fact, because they are formed from alluvial

274   sediments, a particle selection may have occurred, leaving in the soil lithogenic (more resistant to changes)

275   and pedogenic materials (with a higher degree of crystallinity). Unlike the sand fraction, the clay fraction

276    increased gradually with depth, with values from 48 to 558 g kg$^{-1}$. However, we cannot say this is a pedogenic

277    process of eluviation and illuviation. The most likely is the selective removal of surface horizons (more sandy),

278    with clay accumulation in the subsurface.

279    Neosols presented higher proportions of coarse fractions (> 2 mm) of consolidated ferruginous material as

280    plinthite and petroplinthite due to a possible lowering of the water table, leading to a better drainage of the

281    environment, which was confirmed by the presence of a more reddish hue (2.5 YR) in relation to the other

282    profiles from 48 cm from the surface (Table 1). This predominance of coarser sand fractions, together with the

283    marked presence of gravels, are indicative characteristics that the weathering processes in this soil were not

284    able to promote a marked fragmentation of these fractions (EMBRAPA, 2013).

285    In the transport foothill, the clay contents ranged from 95 to 99 g kg$^{-1}$ in the A, AB, and BA horizons to 548

286    g kg$^{-1}$ in the Bt1 horizon, 558 g kg$^{-1}$ in the Bt2 horizon, and 567 g kg$^{-1}$ in the Btf horizon. The marked textural

287    differentiation between the A and Bt1 horizons characterizes an abrupt textural change with a significant

288    increase of clay in relation to the overlying horizons (Table 1).

289    At the top and upper and lower thirds, the silt to clay ratio (S/C) ranged from 1.43 to 1.50 and 1.19 to 1.43,

290    respectively (Table 1), being associated with less developed soils. The transport foothill showed the lowest

291    S/C ratio, with values between 0.7 and 0.8. On the contrary, the deposition foothill presented the highest values

292    (1.49) in the surface horizons but decreasing to 0.41 with variations in depth. According to Campos et al.

293    (2011), higher values of S/C ratio are due to the low increase in the silt fraction or clay loss, suggesting that

294    small relief variations provide relative losses or gains and, possibly, are not motivated by variations in the

295    parent material.

296    Considering the topographic variations, clay and silt contents tended to increase towards the youngest

297    geomorphic surfaces, i.e. from the top and thirds to the transport and deposition foothills, in an opposite

298    direction to that of the total sand, which reflects their recent sedimentary nature since the soils of these

299    geomorphic environments are closely related to the parent material. Campos et al. (2012b) also evidenced this

300    condition when studying the soil-geomorphic surface relationships in a toposequence floodplain-upland in the

301    region of Humaitá, AM, Brazil.

302    **4.3 Variation of chemical attributes**

303    The values of pH ranged from 4.17 to 5.48 (H$_2$O) and 3.81 to 5.70 (KCl), especially in the upper and lower

304   thirds and deposition foothill, presenting the highest acidity content in the surface horizon. According to

305   Campos et al. (2012b), the high regional precipitation contributes significantly to base leaching, increasing

306   soil pH. The balance of negative net charges, expressed by ΔpH in the B horizon, showed the highest values

307   at the top and upper and lower thirds, which is in accordance with the trend of occurring soils with a lower

308   degree of evolution in the youngest surface (Table 2).

309   TABLE 2. Soil chemical attributes in a topolithosequence in Amazonas, Brazil.

| Horizon | pH | | $Ca^{2+}$ | $Mg^{2+}$ | $K^+$ | SB | $Al^{3+}$ | H+Al | CEC | m | V | P resin | OC |
|---|---|---|---|---|---|---|---|---|---|---|---|---|---|
| | $H_2O$ | KCl | - - - - - - - - - - - - - - - - $cmol_c\ dm^{-3}$--- -- - - - - -- | | | | | | | --%-- | | $mg\ dm^{-3}$ | $g\ kg^{-1}$ |
| Top – Leptic Dystrophic Ta Haplic Cambisol – CXvd | | | | | | | | | | | | | |
| A | 4.79 | 3.81 | 1.00 | 0.15 | 0.12 | 1.27 | 4.3 | 19.42 | 21 | 77 | 6 | 4.6 | 59.33 |
| AB | 4.94 | 4.50 | 0.20 | 0.14 | 0.11 | 0.35 | 4.4 | 19.38 | 20 | 93 | 2 | 3.1 | 26.50 |
| Bi | 4.62 | 4.42 | 0.30 | 0.09 | 0.12 | 0.51 | 4.9 | 18.48 | 19 | 91 | 3 | 2.8 | 31.49 |
| BCr | 5.11 | 4.34 | 0.20 | 0.06 | 0.070 | 0.33 | 4.8 | 19.32 | 20 | 94 | 2 | 2.4 | 15.94 |
| Upper third – Leptic Dystrophic Regolithic Neosol – RRd | | | | | | | | | | | | | |
| A | 4.17 | 3.89 | 0.40 | 0.17 | 0.11 | 0.68 | 5.5 | 18.21 | 19 | 87 | 4 | 3.9 | 47.42 |
| ACr | 4.41 | 4.3 | 0.20 | 0.14 | 0.09 | 0.43 | 5.4 | 16.23 | 17 | 91 | 3 | 2.7 | 30.34 |
| Cr/Bi | 5.19 | 4.25 | 0.30 | 0.14 | 0.09 | 0.53 | 5.2 | 14.47 | 15 | 89 | 4 | 2.8 | 26.36 |
| Lower third – Typic Orthic Quartzarenic Neosol – RQo | | | | | | | | | | | | | |
| A | 4.91 | 4.16 | 0.20 | 0.12 | 0.09 | 0.41 | 4.3 | 19.17 | 20 | 91 | 2 | 2.6 | 48.19 |
| $C_1$ | 5.2 | 4.70 | 0.40 | 0.12 | 0.06 | 0.58 | 5.3 | 17.25 | 18 | 90 | 3 | 2.0 | 34.69 |
| $C_2$ | 4.97 | 4.43 | 0.40 | 0.12 | 0.08 | 0.60 | 5.5 | 15.88 | 16 | 90 | 4 | 2.1 | 19.78 |
| $C_3$ | 4.72 | 4.16 | 0.20 | 0.12 | 0.08 | 0.40 | 5.7 | 17.77 | 18 | 93 | 2 | 2.2 | 6.34 |
| Cr | 4.8 | 4.13 | 0.50 | 0.15 | 0.10 | 0.75 | 5.6 | 18.21 | 19 | 88 | 4 | 2.1 | 0.19 |
| Transport foothill – Typic Dystrophic Argiluvic Plinthosol – FTd | | | | | | | | | | | | | |
| A | 4.95 | 3.97 | 0.40 | 0.17 | 0.12 | 0.69 | 3.9 | 26.03 | 27 | 85 | 3 | 3.1 | 51.07 |
| AB | 5.03 | 4.19 | 0.20 | 0.06 | 0.09 | 0.34 | 3.9 | 23.73 | 24 | 92 | 1 | 1.9 | 42.43 |
| BAf | 5.2 | 4.17 | 0.60 | 0.17 | 0.11 | 0.88 | 3.1 | 18.86 | 20 | 78 | 4 | 1.4 | 37.63 |
| Bf | 5.35 | 4.42 | 0.20 | 0.09 | 0.06 | 0.35 | 3.5 | 19.43 | 20 | 91 | 2 | 1.7 | 32.64 |
| BCr | 5.48 | 4.52 | 0.30 | 0.12 | 0.06 | 0.48 | 3.5 | 18.15 | 19 | 88 | 3 | 0.7 | 29.18 |
| Deposition foothill – Abruptic Dystrophic Yellow Argisol – Pad | | | | | | | | | | | | | |
| A1 | 4.23 | 3.88 | 0.30 | 0.15 | 0.13 | 0.58 | 4.3 | 27.72 | 28 | 88 | 2 | 5.8 | 69.89 |
| A2 | 4.33 | 4.06 | 0.70 | 0.12 | 0.10 | 0.92 | 4.3 | 24.98 | 26 | 82 | 4 | 3.3 | 43.39 |
| AB | 4.74 | 4.15 | 0.20 | 0.06 | 0.06 | 0.32 | 4.9 | 18.66 | 19 | 94 | 2 | 2.0 | 37.25 |
| $Bt_1$ | 4.83 | 4.22 | 0.70 | 0.09 | 0.07 | 0.86 | 4.2 | 26.5 | 27 | 83 | 3 | 2.1 | 31.68 |
| $Bt_2$ | 4.8 | 4.25 | 0.60 | 0.17 | 0.06 | 0.84 | 4.6 | 25.86 | 27 | 85 | 3 | 2.2 | 31.49 |
| Btf | 4.23 | 3.88 | 0.30 | 0.15 | 0.13 | 0.84 | 4.9 | 24.73 | 26 | 85 | 3 | 2.1 | 10.67 |

310   SB: sum of bases; CEC: cation exchange capacity; V: base saturation; m: aluminum saturation; OC: organic

311   carbon.

312   The bases $Ca^{2+}$, $Mg^{2+}$, and $K^+$ presented values ranging from 0.20 to 1.0 $cmol_c\ kg^{-1}$ (Table 2). In general, the

313   magnitude of this variation is small among the landscape positions, which is mainly due to their reduced

314   contents in the minerals constituting the sandstone-gneiss and climate conditions that favor the advanced soil

315   weathering in the region. Moreover, the predominance of oxidic minerals generates positive charges, which,

316   allied with the more sandy texture, provided the loss or movement of these cations to subsurface horizons.

317   This behavior, however, does not apply to K, which remained at higher concentrations near the soil surface.

318   According to Neves et al. (2009), this is a characteristic attributed to the low diffusion power electrostatically

319   adsorbed to negative charges of organic matter or the formation of sphere complexes external to the solid

320   phase.

321   Exchangeable aluminum ($Al^{3+}$) content had no marked variation along the topolithosequence, with low values

322   recorded in all profiles, mainly in the A horizon and increasing in depth. In addition, the potential acidity ($H^+$

323   and $Al^{3+}$) values were high and increase in depth along the topolithosequence (Table 2). Possibly, the intense

324   rainy season of the region associated with unimpeded drainage would be the determining climate factors to

325   acidify the soil in depth (Campos et al., 2012).

326   Along the topolithosequence, organic carbon (OC) contents were very higher in the surface horizons because

327   of the concentration of organic matter from the decomposition of native vegetation (Santos et al., 2012). Cation

328   exchange capacity (CEC) ranged from high to very high, with values between 12 and 28 $cmol_c$ $dm^{-3}$. The same

329   trend occurred for the sum of bases (SB), which was higher in the A horizon mainly because of the OM and

330   low clay content, which had low activity.

331   Due to the low activity of the clay fraction, all segments were classified as dystrophic (Table 2). This evidence

332   is a result of the depletion of bases ($Ca^{2+}$, $Mg^{2+}$, and $K^+$), which is in accordance with other investigations

333   developed in the Amazon region (CAMPOS et al., 2012ab; Santos et al., 2012; Martins et al., 2006). This is

334   an interesting aspect since it evidences the Amazon conditions related to the constitution of formation of the

335   parent material associated with weathering conditions of climate, leading the values of base saturation to

336   present a gradient coincident with the geomorphic surfaces, being dystrophic along the topolithosequence.

337   This result is different from those found by Campos et al. (2010), who observed a higher degree of soil

338   development at top positions and dominance of dystrophic soils.

339   Soils were considered alic along the topolithosequence, with values of aluminum saturation (m) ranging from

340   51 to 91%. Martins et al. (2006) studied soils in a transition fields-forest in the region of Humaitá, AM, and

341   also reported the percentage magnitude found here. This is an inherent characteristic of the sandstone-gneiss,

342   which has by nature an acidic character. The richness in Al justifies the formation of gibbsite in the Neosols

343   (upper and lower third), as mentioned.

344 Available phosphorus (P) contents showed a similar behavior along the topolithosequence, with an average of

345 2.0 mg kg⁻¹ and decreasing in depth. Silva et al. (2006) stated that P remains stable in depth due to its low

346 mobility. Another point considered is the strong affinity of iron oxides, mainly goethite in phosphorus retention

347 (Pinto et al., 2013; Rotta et al., 2015). Goethite soils, as is our study, have their P adsorption affinity potentiated

348 because of the high isomorphic substitution (IS) and SSA of Gt. However, the positions at the top and transport

349 and deposition foothills presented values of 4.6 and 5.8 mg kg⁻¹, respectively, of available phosphorus in the

350 A horizon, with the highest values in the topolithosequence. This would be an effect of OM accumulation in

351 the form of litter on the soil surface horizon. In addition, OM acts as a physical barrier, inhibiting the direct

352 contact of P to the soil active sites, thus allowing P in the available soil fraction (Fink et al., 2014).

353 **4.4 Mineralogical attributes**

354 The mineralogy of the clay fraction (Table 3) of diagnostic and transitional B horizons showed the coexistence

355 of the minerals kaolinite (Kt), gibbsite (Gb), hematite (Hm), and goethite (Gt). In a preferred order, Fe oxides,

356 Hm, and Gt predominate as follows: transport foothill (9–41g kg⁻¹) > deposition foothill (5–39 g kg⁻¹) > top

357 (5–24 g kg⁻¹) > upper and lower third (1–5 g kg⁻¹). Among the iron oxides, Gt participated in the clay fraction

358 of all studied soils, which is due to the iron poverty of sandstone-gneiss sediments (Correa et al., 2008; Santos

359 et al., 2010). Under this lithological condition, Gt preferably has its formation favored (Barrón and Torrent,

360 2002; Viscarra Rossel et al., 2010), as shown by the low Hm contents, with a maximum value of 9 g kg⁻¹ in

361 the topolithosequence.

362 TABLE 3. Crystallographic attributes of soil minerals of a topolithosequence in Amazonas, Brazil.

| Soil | MCD | | | | WHH | | SSA | | IS | | Ratio | Content | |
|---|---|---|---|---|---|---|---|---|---|---|---|---|---|
| | °2θ | | | | | | m² g⁻¹ | | mol mol⁻¹ | | | g kg⁻¹ | |
| | Gt₁₁₀ | Gt₁₁₁ | Hm₁₁₀ | Hm₀₁₂ | Kt | Gb | Gt | Hm | Gt | Hm | Kt/(Kt+Gb) | Gt | Hm |
| CXvd_AB | 20.6 | 9.4 | 21.6 | 31.1 | 0.5 | 0.25 | 116.3 | 54.4 | 0.43 | 0.07 | 0.56 | 24 | 5 |
| CXvd_Bi | 15.2 | 8.9 | 16.4 | 54.6 | 0.51 | 0.31 | 159.7 | 79.9 | 0.15 | 0.02 | 0.45 | 21 | 5 |
| RRd_ACr | 25.1 | 18.2 | 25.4 | 28.3 | 0.50 | 0.17 | 94.6 | 41.3 | 0.38 | 0.04 | 0.87 | 5 | 1 |
| RQo_Cr | 25.1 | 13.9 | 12.8 | 36.6 | 0.70 | 0.28 | 94.6 | 89.4 | 0.33 | 0.02 | 0.76 | 5 | 1 |
| FTd_Bf | 18.5 | 14.9 | 22.8 | 30.2 | ni | 0.34 | 130.1 | 47.2 | 0.39 | 0.12 | 0.37 | 41 | 9 |
| FTd_BAf | 10.4 | 7.8 | 15.0 | 89.6 | 0.48 | 0.30 | 234.3 | 78.6 | 0.31 | 0.11 | 0.41 | 40 | 9 |
| PAd_Bf | 23.7 | 11.9 | 13.9 | 63.0 | 0.55 | 0.28 | 100.5 | 77.5 | 0.36 | 0.17 | 0.63 | 39 | 9 |
| PAd_Btf | 28.4 | 21.2 | 17.7 | 49.1 | 0.50 | 0.27 | 82.93 | 63.5 | 0.44 | 0.13 | 0.60 | 25 | 5 |

363 MCD: mean crystal diameter; WHH: width at half-height, SSA: specific surface area, IS: isomorphic

364 substitution; Gt:goethite; Hm: hematite; Kt: kaolinite; Gb: gibbsite; ni: not identified.

365   In general, the crystallographic parameters (MCD, WHH, SSA, and IS) were sensitive to the peculiarities of

366   the topolithosequence (Table 3). The mean crystal diameter (MCD) values for Gt110 (10–28 nm) and Gt111

367   (9–21 nm) peaks lower than Hm111 (12–25 nm) and Hm012 (30–89 nm) peaks revealed the persistence of the

368   crystalline Hm in relation to Gt, a common characteristic in tropical soils (Inda Júnior and Kämpf, 2005;

369   Barbieri *et al.*, 2014) clearly observed in the transport foothill, where peaks referring to the face of Hm012 are

370   well-defined and narrow (Figure 4). The climatic conditions of the Amazon, especially precipitation and

371   temperature, combined with the natural increase of OM, acid pH (Table 2), and intense microbial activity,

372   contribute to a higher presence of Al in the goethite structure, which decreases its crystallinity.
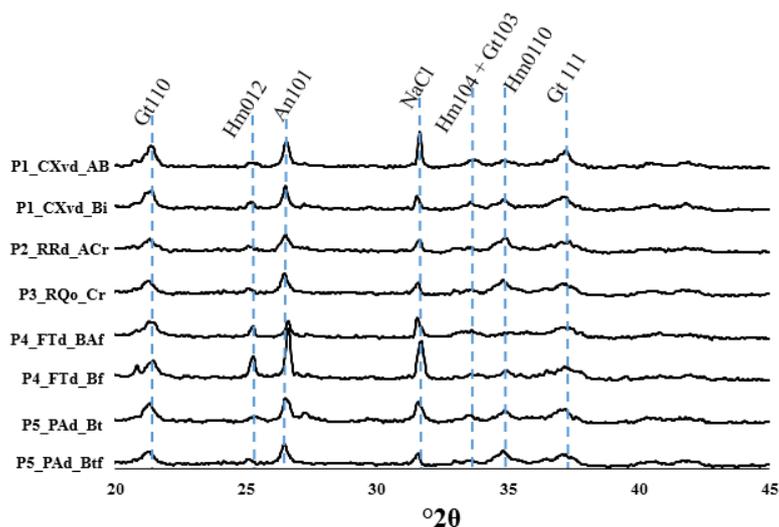
373

374   Figure 4. X-ray diffractograms of the clay fraction for hematite (Hm) and goethite (Gt) in the profiles of Haplic

375   Cambisol (CXvd_AB), Regolithic Neosol (RRd_ACr), Quartzarenic Neosol (RQod_Cr), Argiluvic Plinthosol

376   (FTd_Bf; P4_FTd_BAf), and Yellow Argisol (PAd_Bt; P5_PAd_Btf) in Amazonas, Brazil.

377   Except for the top position, values of isomorphic substitution (IS) higher than 0.33 mol mol$^{-1}$, regardless of

378   the soil position in the topolithosequence, indicate soils with a markedly weathering, non-hydromorphic, and

379   acid pH (high Al activity) (Table 2). These conditions justify the persistence of Gt with a high Fe substitution

380   (r=0.065) by Al (r=0.053), which promoted the contraction of the unit cell and, consequently, increased the

381   specific surface area (SSA), ranging from 82 to 234 m$^2$ g$^{-1}$ in Gt and 41 to 89 m$^2$ g$^{-1}$ in Hm. These results are

382   consistent with those found by other authors in Brazilian soils (Melo et al., 2001; Correa et al., 2008; Carvalho

383   Filho et al., 2015) since the highest values of IS and SSA in Gt are attributed to its higher structural capacity

384   to accommodate Al in relation to Hm (Schwertmann and Taylor, 1989; Rolim Neto et al., 2004).

385   The contents of Fe oxides are concentrated in the soils in the following order: transport foothill > deposition

386   foothill > top > upper and lower third (Table 3 and Figure 4). In turn, the highest contents of Fe oxide,

387   especially Hm in the Plinthosol (P4), are due to an increase of iron in the BAf and Bf horizons, characterized

388   by the presence of ferruginous concretions, which is peculiar to Plinthosols in the study region (Campos et al.,

389   2012). Well-formed peaks of Gt were observed even in poorly developed profiles, as in the case of RQo_Cr,

390   in which the presence of lytic contact (weak rock or outcropping saprolite) is noticeable (Figure 4). This fact

391   was already expected since goethite is the first Fe oxide formed in the early stages of pedogenesis in the initial

392   horizons close to the rock (Curi and Franzmeier, 1984; Silva, 2016).

393   The Kt/(Kt+Gb) ratio showed that Gb is an important constituent of the mineralogical assembly of the studied

394   soils, except for upper and lower thirds and deposition foothill (Table 1 and Figure 5). The lower Kt contents,

395   as well as its absence in the transport foothill, are probably due to the higher iron oxides contents, which may

396   have disrupted Kt nucleation, a behavior also observed in the studies of Gidhin et al. (2006). This resulted in

397   the highest values of width at half-height (WHH), which ranged from 0.483 to 0.703 nm when compared to

398   Gb crystals, which in turn ranged from 0.273 to 0.307 nm. This result indicates that Gb crystals are much more

399   crystalline than Kt, which is soil characteristic with a higher degree of weathering (Gidhin et al., 2006;

400   Camargo et al., 2008), in which the growth of Gb crystals are favored by the low Si concentration in the soil

401   (HSU, 1989).
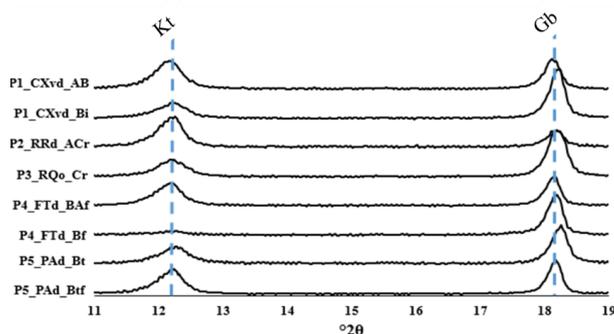
402

403   Figure 5. X-ray diffractograms of the clay fraction for kaolinite (Kt) and gibbsite (Gb) in the profiles of Haplic

404   Cambisol (CXvd_AB), Regolithic Neosol (RRd_ACr), Quartzarenic Neosol (RQod_Cr), Argiluvic Plinthosol

405   (FTd_Bf; P4_FTd_BAf), and Yellow Argisol (PAd_Bt; P5_PAd_Btf) in Amazonas, Brazil.

406   The proportions of Kt[Kt/Kt+Gb > 75], associated with the low iron oxide contents found in Neosol profiles,

407   confirm the lower intensity of pedogenesis or that morphogenesis predominated over the pedogenesis

408   (Scarciglia et al., 2005). Thus, the geomorphological characteristics such as a more rugged and dissected

409   topography of Neosol environments (Figure 3) favored the partial removal of basic cations and silicon, which

410   are combined in the soil to form Kt (Kämpf et al., 2009). In addition, part of this Si and Al removed from the

411   weathering of soils located at the landscape top could have been transported and accumulated in the lower

412   landscape positions, which increased the values of the Kt[Kt/Kt+Gb > 60] ratio in Argisols (P5). These

413   evidences are in accordance with several studies (Curi and Franzmeier, 1984; Ghidin et al.. 2006; Campos et

414   al., 2007; Silva, 2016), which considered the landscape a passive factor of formation and retribution of

415   pedogenic minerals.

416   **5 Conclusions**

417   Landscape separation into compartments and parent material identification were efficient for understanding

418   the variation of soil attributes along the transect.

419   Variations in soil classes are related to topography surfaces and parent material, thus showing variations related

420   to physical, chemical, morphological, and mineralogical attributes.

421   The mineralogy of the clay fraction is composed of kaolinite, goethite, hematite, and gibbsite, with goethite

422   being the predominant iron oxide. In addition, mineralogy confirmed that the chemical properties, especially

423   the cations of exchangeable bases, from sediments originating from these soils were naturally poor in bases

424   and, therefore, not related to the removal process of the system, as it is widely recognized in the Amazon

425   region.

426   A sand fraction dominance was observed in relation to the other fractions in all the surfaces, which is related

427   to the alluvial nature of the parent material, with the highest values occurring in the Quartzarenic Neosol and

428   increasing values as soil profile deepens.

429   **Acknowledgment**

430   Conselho Nacional de Desenvolvimento Científico e Tecnológico (CNPq), Coordenação de Aperfeiçoamento

431   de Pessoal de Nível Superior (CAPES), Fundação de Amparo à Pesquisa no Estado do Amazonas (FAPEAM).

432   **References**

433  Barbieri D. M., Marques Júnior J., Siqueira D.S., Teixeira D.B., Panosso A.R., Pereira G.T., La Scala Junior

434  N. Iron oxides and quality of organic matter in sugarcane harvesting systems. Revista Brasileira de Ciência do

435  Solo. 38, 1143-1152. http://dx.doi.org/10.1590/S0100-06832014000400010, 2014.

436  Barrón V., Torrent J. Evidence for a simple pathway to maghemite in earth and mars soils. Geochimica et

437  Cosmochimica Acta, 66, 2801-2806. https://doi.org/10.1016/S0016-7037(02)00876-1, 2002.

438  Bockheim J.G., Gennadiyev N.A., Hammer R.D., Tandarich J.P. Historical development of key concepts in

439  pedology. Geoderma. 124, 23-36. https://doi.org/10.1016/j.geoderma.2004.03.004, 2005.

440  BRASIL. Ministério das Minas e Energia. Projeto Radam Brasil. Brasil: 1978.

441  Camargo L.A., Marques J.R.J., Pereira G.T., Horvat R. Variabilidade espacial de atributos mineralógicos de

442  um Latossolo sob diferentes formas do relevo. I - Mineralogia da fração argila. Revista Brasileira de Ciência

443  do Solo. 32, 2269–2277. http://dx.doi.org/10.1590/S0100-06832008000600006, 2008.

444  Campos M.C.C. Relações solo-paisagem: conceitos, evolução e aplicações. **Ambiência**, 8: 963-982.

445  doi:10.5777/ambiencia.2012.05.01rb, 2012c.

446  Campos M.C.C., Ribeiro M.R., Souza Júnior V.S., Ribeiro Filho M.R., Almeida M.V. Revista Brasileira de

447  Ciência do Solo. 36: 325 – 336, 2012b.

448  Campos M.C.C., Marques Júnior J., Pereira G.T., Montanari R., Camargo L.A. Relações solo-paisagem em

449  uma litossequência arenito-basalto na região de Pereira Barreto, SP. Revista Brasileira de Ciência do Solo. 31,

450  519-529, 2007.

451  Campos M.C.C., Ribeiro M.R., Souza Júnior V.S., Ribeiro Filho M.R., Costa E.U.C. Segmentos de vertente e

452  atributos do solo de uma topossequência na região de Manicoré, AM. Revista Ciência Agronômica. 41, 501-

453  510, 2010.

454  Campos M.C.C., Ribeiro M.R., Souza Júnior V.S., Ribeiro Filho M.R., Souza R.V.C. Relações solo-paisagem

455  em uma topossequência sobre substrato granítico em Santo Antônio do Matupi, Manicoré (AM). Revista

456  Brasileira de Ciência do Solo. 35, 13-23. http://dx.doi.org/10.1590/S0100-06832011000100002, 2011.

457  Campos M.C.C., Ribeiro M.R., Souza Júnior V.S., Ribeiro Filho M.R., Souza R.V.C.C., Almeida M.C.

458  Topossequência de solos na transição Campos Naturais-Floresta na região de Humaitá, Amazonas. Acta

459  Amazônica. 42, 387-398. http://dx.doi.org/10.1590/S0044-59672012000300011, 2012a.

460  Carvalho Filho A., Inda Júnior A.V., Fink J.R., Curi N. Iron oxides in soils of different lithological origins in

461 Ferriferous Quadrilateral (Minas Gerais, Brazil). Applied Clay Science. 118, 1–75.

462 https://doi.org/10.1016/j.clay.2015.08.037, 2015.

463 Correa M.M., Ker J.C., Barrón V., Fontes M.P.F., Torrent J., Curi N. Caracterização de óxidos de ferro de

464 solos do ambiente tabuleiros costeiros. Revista Brasileira de Ciência do Solo. 32, 1017-1031.

465 http://dx.doi.org/10.1590/S0100-06832008000300011, 2008.

466 CPRM, Serviço Geológico do Brasil. Centro de Pesquisa de Recursos Minerais. Hidroclimatologia, geologia,

467 recursos minerais, geomorfologia e unidades de paisagens. Relatório Técnico. Manaus: 2001.

468 Curi N., Franzmeier D.P. Toposequence of Oxisols from the Central Plateau of Brazil. Soil Science Society

469 America Journal. 48, 341- 346. doi:10.2136/sssaj1984.03615995004800020024x, 1984.

470 Dalamerlinda E.A., Souza Júnior V.S., Wadt P.G.S., Deng Y., Campos M.C.C., Câmara, E.R.G. Soil-

471 landscape relationship in a chronosequence of the middle Madeira River in southwestern Amazon, Brazil.

472 Catena. 149: 199-208. https://doi.org/10.1016/j.catena.2016.09.021, 2017.

473 Dalrymple J.B., Blong R.J., Conacher A.J. A hypothetical nine unit landsurface model. Z. Geomorphology.

474 12, 60-76, 1968.

475 Donagema G.K., Campos D.V.B., Calderano S.B., Teixeira W.G., Viana J.H.M. Manual de métodos de análise

476 de solo. 3nd ed. Rio de Janeiro: Embrapa Solos, 2017.

477 Fink J.R., Inda A.V., Bayer C., Torrent J., Barrón V. Mineralogy and phosphorus adsorption in soils of south

478 and central-west Brazil under conventional and no-tillage systems. Acta Science Agronomic. 36, 379–387.

479 http://dx.doi.org/10.4025/actasciagron.v36i3.17937, 2014.

480 Ghidin A.A., Melo V.F., Lima V.C., Lima J.M.J.C. Topossequências de latossolos originados de rochas

481 basálticas no paraná. I – Mineralogia da fração argila. Revista Brasileira Ciência Solo. 30, 293-306.

482 http://dx.doi.org/10.1590/S0100-06832006000200010, 2006.

483 Hsu P.H., Dixon J.B., Weed S.B. In: Aluminiun oxides and oxyhydroxides. eds. Minerals in soil environments.

484 2nd ed. Madison; Soil Science Society of America: 331- 378. 1989.

485 Inda Júnior A.V, Kämpf N. Variability of goethite and hematite via reductive dissolution in soils of the tropical

486 and subtropical. Revista Brasileira Ciência Solo. 29, 851-866. http://dx.doi.org/10.1590/S0100-

487 06832005000600003, 2005.

488 Kämpf N. Die Eisenoxidmineralogie einer Klimasequenz von Böden aus Eruptiva in Rio Grande do Sul,

489    Brasilien. Doctoral thesis. Freising, Technische Universitat München, Munique, 1981.

490    Kämpf N, Curi N, Marques J.J. Óxidos de alumínio, silício, manganês e titânio. In: Melo, V.F. and Alleoni

491    L.R.F. Química e mineralogia do solo. Viçosa: Sociedade Brasileira de Ciência do Solo, 2000.

492    Kämpf N, Curi N. Tópicos em ciência do solo - óxidos de ferro: Indicadores de ambientes pedogênicos e

493    geoquímicos. Viçosa: Sociedade Brasileira de Ciência do Solo, 2000.

494    Klug H.P., Alexander L.E. X-Ray Diffraction Procedures for Polycrystalline and Amorphous Materials. New

495    York: Wiley, 1974.

496    Kroth P.L. Disponibilidade de fósforo no solo para plantas e fatores que afetam a extração por resina de troca

497    em membrana. Universidade Federal do Rio Grande do Sul, Porto Alegre, 1988.

498    Li Z.W., Zhang G.H., Geng R., Wang H. Rill erodibility as influenced by soil and land use in a small watershed

499    of the loess plateau, China. Biosystems Engineering. 129, 248-257.

500    https://doi.org/10.1016/j.biosystemseng.2014.11.002, 2015.

501    Marques Júnior J., Lepsch I.F. Depósitos superficiais neocenozóicos, superfícies geomórficas e solos em

502    Monte Alto, SP. Geociências. 19, 90-106, 2000.

503    Martins G.C., Ferreira M.M., Curi M., Vitorino A.C.T., Silva M.L.N. Campos nativos e matas adjacentes da

504    região de Humaitá (AM): atributos diferencias dos solos. Ciência e Agrotecnologia. 30, 221-227.

505    http://dx.doi.org/10.1590/S1413-70542006000200005, 2006.

506    Mehra O.P., Jackson M.L. Iron oxide removal from soils and clays by a dithionite-citrate system buffered with

507    sodium bicarbonate. In: Swineford A. National conference on clays and clay mineral. Pergamon Press,

508    Washington, 317–342. https://doi.org/10.1016/B978-0-08-009235-5.50026-7, 1960.

509    Melo V.F, Fontes M.P.F., Novais R.F., Singh B., Schaefer C.E.G.R. Caracterização dos óxidos de ferro e de

510    alumínio de diferentes classes de solos. Revista Brasileira de Ciência do Solo. 25, 19-32.

511    http://dx.doi.org/10.1590/S010006832001000100003, 2001.

512    Minasny B., Mcbratney A.B. Mechanistic soil-landscape modelling as an approach to developing pedogenetic

513    classifications. Geoderma. 133, 138-149. https://doi.org/10.1016/j.geoderma.2006.03.042, 2006.

514    Montanari R., Marques Júnior J., Campos M.C.C., Souza Z.M., Camargo L.A. Caracterização mineralógica

515    de Latossolos em diferentes feições do relevo na região de Jaboticabal, SP. Revista Ciência Agronômica. 41,

516    191-199, 2010.

517 Murphy J., Riley J.P.A. Modified single solution method for the determination of phosphate in natural waters.

518 Anal Chimica Acta. 27, 31-36. https://doi.org/10.1016/S0003-2670(00)88444-5, 1972.

519 Neves, C.M.N., Silva, M.L.N., Curi, N., Macedo, R.L.G., Moreira, F.M.S., Norrish K., Taylor R.M. The

520 isomorphous replacement of iron by aluminum in soil goethites. Journal Soil Science. 12, 294–306.

521 https://doi.org/10.1111/j.1365-2389.1961.tb00919.x, 1961.

522 Pinto F.A., Souza E.D., Paulino H.B., Curi N., Carneiro M.A.C.P.: P-sorption and desorption in Savanna

523 Brazilian soils as a support for phosphorus fertilizer management. Ciência e Agrotecnologia. 37, 521-530.

524 http://dx.doi.org/10.1590/S1413-70542013000600005, 2013.

525 Ribeiro M.R., Oliveira L.B., Araujo Filho J.C., Ker J.C., Curi N., Schaefer C.E.G.R., Vidal-Tornado P.

526 Caracterização Morfológica do solo. eds. Pedologia; fundamentos, 2012.

527 Rotta L.R., Paulino H.B., Anghinoni I., Souza E.D., Carneiro M.A.C. Phosphorus fractions and availability in

528 a haplic plinthosol under no-tillage system in the brazilian cerrado. Ciência e Agrotecnologia. 39, 216-224.

529 http://dx.doi.org/10.1590/S1413-70542015000300002, 2015.

530 Santos A.C., Pereira M.G., Anjos L.H.C., Bernini T.A., Cooper M., Nummer A.R., Francelino M.R. Gênese e

531 classificação de solos numa toposseqüência no ambiente de mar de morros do médio Vale do Paraíba do Sul,

532 RJ. Revista Brasileira de Ciência do Solo. 34, 1297-1314. http://dx.doi.org/10.1590/S0100-

533 06832010000400027, 2010.

534 Santos H.G., Jacomine P.K.T., Anjos L.H.C., Oliveira V., Lumberas J.F., Coelho M.R., Almeida J.A., Cunha

535 T.J.F., Oliveira J.B. Centro Nacional de Pesquisa de Solos. Sistema Brasileiro de Classificação de Solos.

536 Brasília, 353p, 2013.

537 Santos L.A.C., Campos M.C.C., Costa H.S., Pereira A.R.: Caracterização de solos em uma toposseqüência

538 sob terraços aluviais na região do médio rio Madeira (AM). Ambiência - Revista do Setor de Ciências Agrárias

539 e Ambientais. 8, 319-331. doi:10.5777/ambiencia.2012.02.07, 2012.

540 Santos R.D., Lemos R.C., Santos H.G., Ker J.C., Anjos L.H.C., Shimizu S.H.: Manual de descrição e coleta

541 de solos no campo. 6nd ed. Viçosa: Sociedade Brasileira de Ciência do Solo, 2013.

542 Scarciglia F., Pera E., Critelli S.: Weathering and pedogenesis in the Sila Grande Massif (Calabria, South

543 Italy): from field scale to micromorphology. Catena. 61, 1–29. https://doi.org/10.1016/j.catena.2005.02.00,

544 2005.

545 Schiavo J.A., Pereira M.G., Miranda L.P.M.D., Neto D., Hypólitom A., Fontana A.: Caracterização e

546 classificação de solos desenvolvidos de arenitos da formação Aquidauana-MS. Revista Brasileira de Ciência

547 do Solo. 3, 881-889. http://dx.doi.org/10.1590/S0100-06832010000300029, 2010.

548 Schulze D.G., Schwertmann U.: The influence of aluminium on iron oxides: X. Properties of Al-substituted

549 goethites. Clay Miner. 19, 521–539. https://doi.org/10.1180/claymin.1984.019.4.02, 1984.

550 Schwertmann U., Kampf N.: The effect of environments on iron oxide minerals. Advances Soil Science. 1,

551 172–200, 1985,

552 Schwertmann U., Taylor R.M.: Iron oxides. In: Dixon JB, Weed SB. Minerals in soil environments. 2nd ed.

553 Soil Science Society of America, Madison, 379–438, 1989.

554 Silva L. S.: Mineralogia da fração argila dos solos do Planalto Ocidental Paulista [dissertação]. Jaboticabal:

555 Faculdade de Ciências Agrárias e Veterinária, Universidade Estadual Paulista (UNESP), 2006.

556 Silva M.B., Anjos L.H.C., Pereira M.G., Nascimento R.A.M. Estudo de toposseqüência da baixada litorânea

557 fluminense: Efeitos do material de origem e posição topográfica. Revista Brasileira Ciência Solo. 25, 965-976.

558 http://dx.doi.org/10.1590/S0100-06832001000400019, 2001.

559 Skogley O., Dobermann A. Synthetic Ion-exchange Resins: Soil and envinonmental studies. Journal of

560 Enviromental Quality. 25, 13-24. doi: 10.2134/jeq1996.00472425002500010004x, 1996.

561 Sommer M.: Influence of soil pattern on matter transport in and from terrestrial biogeosystems - A new concept

562 for landscape pedology. Geoderma. 133; 107–123. doi: 10.1016/j.geoderma.2006.03.040, 2006.

563 Vasconcelos V., Carvalho Júnior A.O., Martins E.S., Couto Júnior A.F., Guimaraes R.F., Gomes R.A.T.;

564 Sistema de classificação geomorfométrica baseada em uma arquitetura sequencial em duas etapas: árvore de

565 decisão e classificador espectral, no Parque Nacional da Serra da Canastra. Revista Brasileira

566 Geomorforfologia. 13, 171–186, 2012.

567 Rossel R.A.V., Rizzo R., Dematte J.A.M., Behrens T.: Spatial modeling of a soil fertility index using visible-

568 near-infrared spectra and terrain atributes. Soil Science Society of America Journal. 74, 1293-130. doi:

569 10.2136/sssaj2009.0130, 2010.

570 ZEE - Zoneamento Ecológico Econômico Do Sul-Sudeste Do Amazonas, Am. (2008) Zoneamento Ecológico

571 Econômico do Sul-Sudeste do Amazonas. Manaus: IPAAM.